COMMUNICATION

The Critical Role of Water Content in the Electrolyte on the Reversible Electrochemical Performance of Zn-VPO_4F Cell†

Hooman Yaghoobnejad Asl, [a] Shyam Sharma [a] and Arumugam Manthiram *[a]

Received 00th January 20xx,
Accepted 00th January 20xx

DOI: 10.1039/x0xx00000x

Abstract. The electrochemistry of the Zn — VPO_4F system has been studied for the first time in both wet non-aqueous and aqueous zinc-ion electrolytes. It is shown that H^+ ions present in the electrolyte insert into the cathode host in preference to the sluggish Zn^{2+} ion insertion. Furthermore, it is demonstrated that while H_2O as a source of the H^+ is essential for proper cell operation, an aqueous electrolyte is detrimental to cathode stability due to extensive dissolution.

Reversible electrochemical energy storage based on multivalent metallic anodes constitutes an interesting platform in secondary batteries.[1–6] The main reason for the interest lies in the high terrestrial abundance of multivalent metals and the possibility of directly implementing these metals as high energy density anodes. However, the major obstacle to the development of such batteries is the lack of insertion hosts as cathodes that can accommodate the multivalent ions through solid-state diffusion. Oxide, sulfide, polyanionic, and Prussian Blue electrodes have been investigated as major categories of solid-state insertion-reaction cathodes for multivalent ions.[7–9]

A related, though fundamentally different, approach to implementing multivalent-ion batteries is via the concept of aqueous electrolytes.[10–12] So far, this strategy has been successfully applied to the design of reversible batteries incorporating zinc as an anode. This is because water is chemically compatible with metallic zinc, although using an aqueous electrolyte comes at the cost of limiting the anodic stability window. An advantage of using aqueous electrolytes is that H^+ is introduced into the electrochemical picture so that the fast diffusing H^+ ions can compensate the electron-transfer charges within the cathode instead of the sluggish Zn^{2+} cation. This has enabled a variety of H^+ or Zn^{2+}/H^+ co-insertion reactions in some polyanionic and oxide-based cathodes.[13–16] Apart from H^+ introduction, aqueous electrolytes can occasionally trigger unwanted electrode-electrolyte side reactions that further complicates the basic insertion chemistry. Therefore, as it will be demonstrated, deconvolution of the Zn^{2+}/H^+ co-insertion, roles of H_2O as a source of H^+ ions, and as a solvent is of crucial importance when dealing with aqueous electrolytes.

Within the class of polyanionic hosts, the tavorite-type vanadium fluoride phosphate VPO_4F is a promising candidate due to its high-voltage, low-polarization, and the ability to undergo more than a single electron redox reaction per transition-metal ion in Li-ion cells.[17] As a multivalent host, however, little work has been done on VPO_4F. Wu *et al*. calculated that VPO_4F can offer a 0.7 eV ionic diffusion pathway for Mg^{2+} ions,[18] although this has yet to be demonstrated experimentally. Furthermore, the behavior of the Zn — VPO_4F system has not been reported previously, either

[a] *Materials Science and Engineering Program and Texas Materials Institute, The University of Texas at Austin, Austin, Texas 78712, United States. *Email: rmanth@mail.utexas.edu*

†Electronic Supplementary Information (ESI) available: Details of syntheses and processing, materials characterization, and electrochemical testing. See DOI: 10.1039/x0xx00000x

in aqueous or non-aqueous electrolytes. Herein, we attempt to study the Zn — VPO_4F system in two different electrolytes, *viz*., a "wet" zinc chloride-urea eutectic melt and an aqueous zinc sulfate electrolyte. The target of this study is two-fold: first, to show that proton is the actual working ion that inserts into the cathode. Second, and more importantly, to demonstrate that while water as a source of H^+ is an essential component of this system, having too much water as in an aqueous electrolyte leads to serious capacity fading due to extensive material dissolution. The result of this work is expected to encourage the scientific community to revisit cathodes that were discarded on the basis of a lack of stability in aqueous Zn-ion cells.

The host VPO_4F was prepared first in the lithiated form through a previously reported two-step solid-state reaction (Figure S1).[19] The obtained host was subsequently delithiated with NO_2BF_4. Figure 1 demonstrates the refined X-ray diffraction pattern of the VPO_4F host, indicating the presence of a maximum of 4 % wt. of $LiVPO_4F$ within the sample after delithiation.

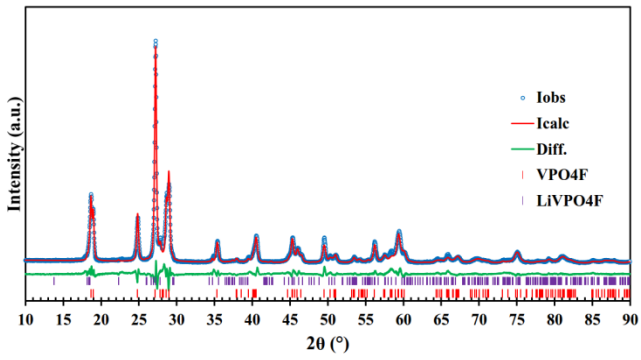

Figure 1. Rietveld refinement on the XRD pattern of the VPO_4F (96 % wt.) phase obtained after the chemical delithiation of $LiVPO_4F$ (4% wt.).

Details of the electrode preparation and the setup used for carrying out the electrochemical studies are described in the Supporting Information. A deep eutectic melt comprising $ZnCl_2$ — $(NH_2)_2CO$ (mole ratio 1 : 3.5) was used as the non-aqueous electrolyte, as reversible electroplating of Zn in this system has been demonstrated previously (Figure S4).[20] To reduce the viscosity of the electrolyte and increase the ionic conductivity within the electrolyte, the electrochemical cells were operated at a constant temperature of 55 °C. Despite the extensive drying procedure undertaken to remove residual moisture from the components of the electrolyte, we suspect that some moisture is always present in the electrolyte due to the deliquescent nature of $ZnCl_2$, making it a wet electrolyte. The amount of the moisture present in the as-prepared electrolyte has been quantified at 493 ppm (details are given in the SI, along with Figure S5). Thus, H^+ could potentially be involved in the charge balance of the redox reactions. Nonetheless, it should be mentioned that due to the abundant Zn^{2+} species (mole fraction: 0.22 as $ZnCl_2$) and the elevated temperatures employed, Zn^{2+} insertion into VPO_4F is also possible should this process be thermodynamically and kinetically favorable.

The galvanostatic charge-discharge curves of the Zn — VPO_4F system at C/50 is shown in Figure 2a. Surprisingly, VPO_4F shows a very well-defined, reversible voltage profile in the ionic liquid electrolyte.

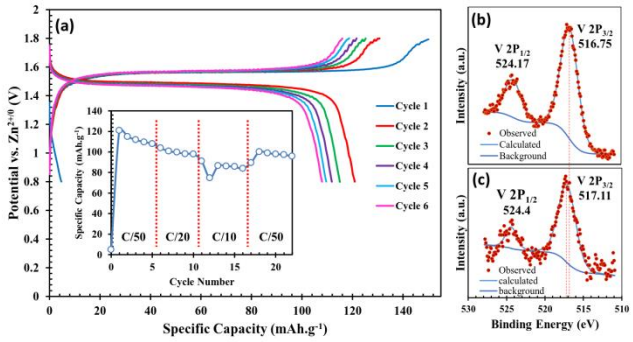

Figure 2. (a) Galvanostatic charge-discharge curves of the Zn - VPO_4F system obtained at a rate of C/50 in zinc chloride/urea ionic liquid electrolyte. The inset shows the higher C rate performance. Core-level XPS spectra of the V 2P transitions, respectively, after discharging (b) and charging (c) the electrode vs. a Zn anode.

After charging the cell to 1.8 V at an average potential of 1.6 V, the discharge curve sweeps through a mostly flat regime delivering a specific discharge capacity of 120 $mAh.g^{-1}$ at an average potential of 1.50 V. Following the first cycle irreversible capacity loss of 20 $mAh.g^{-1}$, the discharge capacity only decays slowly with the cycle number onward, suggesting the reversibility of the core redox reaction. The eventual loss of capacity in this system can be assigned to the slow dissolution of the active material in the electrolyte.

Also, the slow decomposition of the electrolyte can contribute to this capacity loss. Considering the insertion potential and the relative Fermi positions of the Zn and Li metals, the observed discharge potential in Figure 2a translates to + 3.74 V vs. Li^+/Li (ignoring the activity coefficients and temperature difference), which is significantly lower than that for Li^+ insertion into VPO_4F (4.24 V vs. Li^+/Li).[17] Thus, we can suggest that the host-guest interactions under the above experimental conditions are thermodynamically less stable than the analogous Li — VPO_4F system by roughly 0.5 eV per formula unit. Recently, it has been shown that while keeping the Li^+ (de)insertion in VPO4F as the cathodic reaction, the potential of the cell in a hybrid Zn-anode cell yields 1.9 V (vs. $Zn^{2+/0}$).[21] This observation corroborates with the above hypothesis regarding the potential for (de)insertion of H^+ in the $VPO4_F$ host.

The core-level XPS spectra of the vanadium species in the discharged and charged electrodes are shown, respectively, in Figure 2(b) and (c). The V $2P_{3/2}$ transition initially observed at a binding energy of 517.11 eV in the charged cathode shifts to 516.75 eV after discharging the electrode to 0.8 V, indicating the reduction of the V oxidation state from +4 to +3 and the electroactive nature of V in this system.[22–24]

At a first glance, the observed electrochemical performance in the Zn — VPO_4F system may be ascribed to the bulk intercalation of Zn^{2+} into the vanadium phosphate fluoride lattice. However, for some reason that will follow, this seems not to be the case. The galvanostatic intermittent titration (GITT) curve for the entire charge and discharge is presented in Figure 3. There is an apparent charge leakage in the system, either due to the electroactive impurities within the electrolyte that shuttle between the electrodes, or the lack of anodic stability of the electrolyte that causes the charge capacity to be larger than the discharge capacity by about 15%. The flat nature of the quasi-open circuit potential (qOCV) curve and the small polarization between the charge and discharge curves points to the narrow solubility gaps between the cathode redox couple and the small structural hysteresis as a result of cation (de)insertion into the VPO_4F host. The low solubility gap between the oxidized and reduced states of VPO_4F demonstrates the two-phase voltage composition behavior, while the low hysteresis indicates the kinetically facile phase transformation and cation (de)insertion.[25,26] These features are generally contradictory to the insertion chemistry of multivalent cations in solid-state hosts. Typically, the strong coulombic interactions between the host-guest and guest-guest species lead to long-range cation ordering and voltage hysteresis during electrochemical cycling.[27,28]

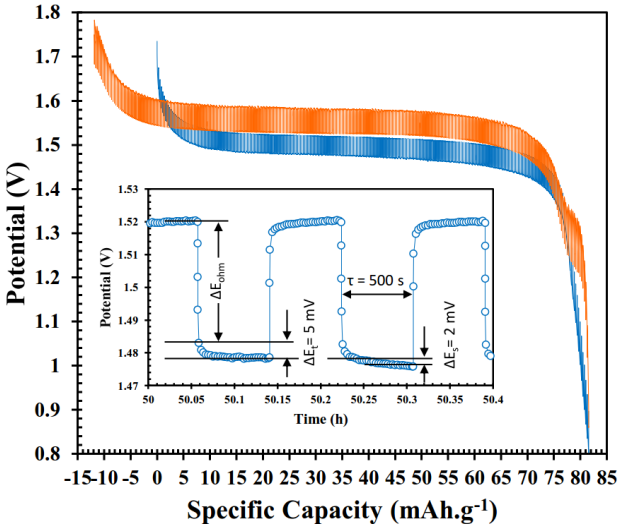

Figure 3. The full-cycle GITT curve of the Zn – VPO_4F system starting from the charged state. The inset shows an expanded view of the discharge titration curve, indicating the values for the parameters used in the equation (1).

From the expanded view of the GITT curve (Figure 3, inset), it can be seen that most of the polarization during the current pulse is due to the Ohmic drop, originating from the ionic conductivity within the electrolyte. The magnitude of the effective diffusion coefficient of the cation can be estimated from the GITT curves according to the equation (1), provided that a sufficiently small titration increment is employed:[29]

$$\widetilde{D} = \frac{4L^2}{\pi\tau}\left(\frac{\Delta E_s}{\Delta E_t}\right)^2 \qquad (1)$$

where $\widetilde{D}$ is the diffusion coefficient ($cm^2.s^{-1}$), L is the linear diffusion length (cm), τ is the current pulse time (s), and ΔE_s and ΔE_t are, respectively, the change in the potential due to the change in the composition of the

electrode between the two sequential titration steps and the overpotential due to mass-transfer resistance within the electrode. Assuming an average effective diffusion length of 500 nm for the cathode particles (SEM provided in Figure S6), equation (1) yields a diffusion coefficient of on the order of 10^{-12} $cm^2.s^{-1}$ for the above system. This value is comparable to the values obtained for the diffusion of Li^+ in VPO_4F cathode,[30,31] and is, therefore, larger than the values anticipated for the diffusion of Zn^{2+} within the tavorite structure. Therefore, we concluded that the moisture present in the ionic-liquid acts as a source of protons that are inserted into the lattice, similar to some previous studies.[13,16] As such, this electrochemical system can be classified as a hybrid cell with the following half-cell reactions:

Anode: $\frac{1}{2}\ Zn_{(s)} + H_2O_{(sol)} \leftrightharpoons \frac{1}{2}\ Zn(OH)_{2(s)} + e^- + H^+_{(sol)}$

Cathode: $VPO_4F_{(s)} + x\ e + x\ H^+_{(sol)} \leftrightharpoons H_xVPO_4F_{(s)}$ (2)

The capacity retention as a function of C rate for the Zn — VPO_4F system is depicted in the inset to Figure 2, showing an observed stable capacity of about 84 $mAh.g^{-1}$ at C/10 rate, compared with 100 $mAh.g^{-1}$ at C/50 rate. The decent higher C-rate performance of this cathode also points to the fact that fast-diffusing protons probably compensate for the electron-transfer rather than Zn^{2+}.

To validate the hypothesis of protons acting as the working ions, the VPO_4F host was subjected to several tests. First, it was realized that the delithiated VPO_4F host prepared through chemical oxidation has the affinity to insert protons topotactically through a spontaneous reaction with atmospheric moisture. All the cells assembled in the presumably charged state delivered a negligible capacity in their first discharge. On the other hand, a large charging capacity equivalent to 150 $mAh.g^{-1}$ could be obtained during the first oxidation (Figure 2(a)) from the pristine electrodes. Also, the first-charge potential curve superimposes perfectly over the subsequent cycles, indicating the identical nature of these electrochemical processes. The XRD powder pattern of the aged VPO_4F sample used for the fabrication of the cathodes is shown in Figure 4, along with the oxidation state analysis of the V species by iodometric titration (inset in Figure 4).

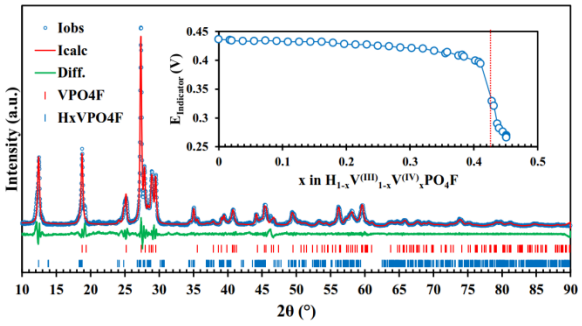

Figure 4. XRD pattern and Pawley refinement of the mixture of phases obtained from VPO_4F powder aged under ambient conditions. The inset shows the oxidation state analysis of the vanadium species by iodometric titration.

Compared to Figure 1, VPO_4F undergoes structural changes as noted by the emergence of a new peak at $2\theta = 12.46°$, while some of the features due to the pristine VPO_4F are still present. Since a meaningful Rietveld refinement is not possible due to the lack of a structural model, a Pawley refinement was attempted here. Due to the systematic absence of the h00, 0k0 and 00l (h, k, l = 1) reflections in the *C 2/c* space group of VPO_4F, the chemically reduced VPO_4F (denoted as $H_xVPO_4F(c)$), has been indexed in a triclinic crystal system (Space Group *P -1*) to account for all the observed diffraction lines. The obtained refined lattice constants of the $H_xVPO_4F(c)$ are a = 7.4563(1) Å, b = 7.1950(9) Å, c = 7.4550(3) Å, α = 91.27(1) °, β = 120.42(8) °, γ = 89.11(1) °, V = 344.77(8) $Å^3$. Comparing $H_xVPO_4F(c)$ with the pristine VPO_4F (V = 323.42(3) $Å^3$) indicates that the reduction of VPO_4F is accompanied by a 6.6 % expansion in the cell volume. Also, the fact that a different space group is required to account for all the observed peaks for a mixture of $H_xVPO_4F(c)$ and VPO_4F indicates that the reduction of VPO_4F to H_xVPO_4F is a biphasic reaction according to equation (3), similar to the observed electrochemical results (Figure 2).

$VPO_4F_{(monoclinic)} + x/2\ H_2O_{(g)} \rightarrow H_xVPO_4F_{(triclinic)} + x/4\ O_{2(g)}$ (3)

The result of the oxidation state analysis by iodometric titration (Figure 4 inset) also suggests an average formula of $H_{0.57}VPO_4F$, confirming the spontaneous

reduction of VPO_4F and corroborating the XRD observations.

In an attempt to confirm whether the same phase transformation occurs as a result of electrochemically reducing VPO_4F in a Zn — VPO_4F system, a large cell incorporating ~ 80 mg of VPO_4F was inspected by *ex situ* XRD after a charge and discharge to, respectively, 1.8 and 0.8 V, as shown in Figure S7. Interestingly, the discharged electrode herein referred to H_xVPO_4F(ec), exhibits the low-angle diffraction line similar to H_xVPO_4F(c), further shifted to $2\theta = 11.68$ °, indicating an even larger lattice. The larger crystal lattice observed can be assigned to the higher degree of VPO_4F protonation as a result of applying an external electrochemical driving force. Also, charging the electrode back to 1.8 V removes the low-angle peak and restoration of the VPO_4F phase, although with severe peak broadening. The observed peak broadening could be due to the crystallite size reduction during the first cycle. Also, the insertion of H^+ in the VPO_4F host can induce internal stress and local structure disorder as a result of hydrogen bonding between oxygen atoms of the phosphate group and the highly electronegative fluoride. A calculated bond valence sum (BVS) map for possible positions of H^+ in the VPO_4F host is given in Figure S8.

Finally, element-specific chemical analyses were employed, aiming to probe the presence of Zn species in the bulk electrode after electrochemical reduction. It is worth noting that zinc hydroxide and its derivatives have a low solubility in polar solvents, often forming solid deposits on the surface of the electrodes. Therefore, without a thorough electrode clean-up step to eliminate zinc deposits from the surface, a chemical analysis may yield false-positive results. Here, the electrodes were first washed with copious amounts of deionized water (DI) to completely dissolve the high-viscosity ionic liquid, sonicated in a 0.01 M HCl solution for 20 min, and washed again with DI water.

The energy dispersive X-ray spectrum (EDXS) of the VPO_4F electrode, following a reduction to 0.8 V vs. Zn^{2+}/Zn, is shown in Figure 5, presenting an estimate of the surface composition of the discharged electrode.

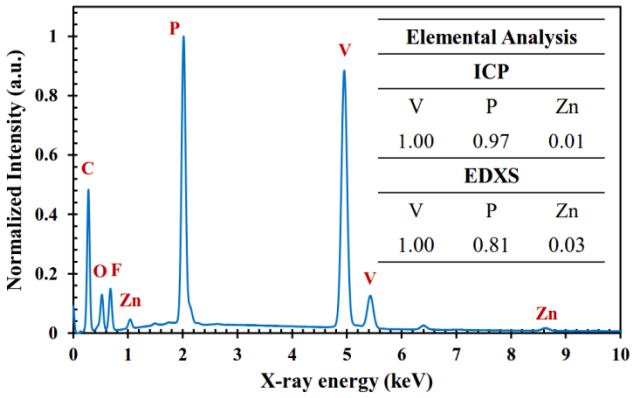

Figure 5. EDS X-ray spectrum of the VPO_4F electrode discharged to 0.8 V vs. Zn metal. The inset shows the quantification results obtained from ICP-OES and EDS.

All the observed peaks were assigned to a carbon-coated VPO_4F electrode, with the electrolyte-specific atoms (N, Cl) absent. Notoriously, very weak K and L line intensities of Zn were observed in the discharged electrode. The results of a semi-quantitative analysis yield an atomic ratio of V : P : Zn equal to 1.0 : 0.81 : 0.03. The relatively high V : P ratio can be assigned to the partial dissolution of the VPO_4F electrode and the accumulation of vanadium species on the surface of the electrode. Nonetheless, the low atomic ratio of Zn in comparison to V and P indicates that Zn^{2+} was virtually absent throughout the discharge process. This was further verified through atomic emission spectroscopy, where the obtained V : P : Zn molar ratio of 1.00 : 0.97 : 0.01 indicates the negligible bulk concentration of Zn in the discharged electrode (Figure S9).

Given that protons play a major role in charge compensation during the electrochemical cycling of the Zn — VPO_4F system, we decided to test the feasibility of operating this system in an aqueous 1.0 M $ZnSO_4$ electrolyte that is an abundant source of H^+ ions. These results are presented in Figure 6. Several subtle differences can be observed when the Zn — VPO_4F system is cycled in an aqueous electrolyte in comparison to the $ZnCl_2$-urea ionic liquid. During the first discharge, the topotactic biphasic insertion reaction shrinks, and eventually, the flat voltage profile

yields into a sloppy regime till reaching the lower cut-off voltage value of 0.8 V. Also, the charge curve shifts to a higher value and becomes sloped.

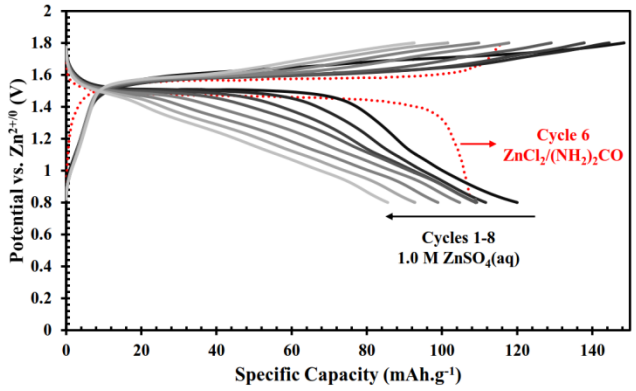

Figure 6. Galvanostatic charge-discharge curves of the Zn – VPO_4F system obtained with 1.0 M $ZnSO_4$(aq) electrolyte at C/20. The 6th cycle of an identical system in the ionic liquid electrolyte is provided for a comparison.

Furthermore, the capacity fade upon continuous cycling is considerably faster than that observed in the ionic liquid electrolyte. The capacity loss correlates with the eventual yellow discoloration observed in the electrolyte, indicating the presence of vanadium species in the electrolyte. All in all, these observations address the unstable electrochemical cycling of VPO_4F in an aqueous electrolyte, most likely due to the dissolution of the protonated VPO_4F in water. It is likely that the change in the nature of the voltage profile from two-phase to mono-phasic reaction originates from a fundamental change in the nature of the electrochemical active phase as a result of dissolution/precipitation. In general, hydrated vanadium oxyhydroxide phases are formed as a result of the VPO_4F reaction with water.

Therefore, one can conclude that despite the essential role that H_2O plays as a source of protons, using aqueous solvents may invariably cause electrode-electrolyte side reactions. As the activity of H_2O in the wet ionic liquid electrolyte is reduced significantly as a result of strong solvation by the solvent ions,[32] water does not interact extensively with the VPO_4F host, thus allowing for longer cell cycle-life.

The opposing roles that H_2O plays in Zn – VPO_4F system with wet ionic liquid electrolyte are somehow contradictory to some of the previously studied cases advocating the presence of electrolyte water for smooth insertion reactions involving hydrated Zn^{+2} ions. In some open structures, such as the layered $VOPO_4.2H_2O$,[33] bi-layer $V_2O_5.nH_2O$,[34] layered $MnO_2.nH_2O$,[35] and Birnessite $MnO_2.nH_2O$,[36] the presence of H_2O in the electrolyte or the structure has been associated with the improved electrochemical performance. This is mainly because (a) these structures have crystalline water that consolidates the structure and (b) their open-framework structure can accommodate hydrated multivalent cations. In addition, the dissociation of H_2O into H^+ and OH^-/O^{-2} and formation of metal oxy-hydroxides may contribute to the facile electrochemical behavior. Thus, the presence of H_2O not only reinforces the structure of the solid, but also participates directly via H^+ generation, or indirectly by screening the host-guest coulombic attractions, allowing for faster insertion kinetics. This is different from the current case study, where H_2O is not part of the structure and undergoes reactions with the host, but at the same time being the source of the H^+ charge carriers. Therefore, depending on the specific case and structural and chemical features of the host, H_2O can play various roles in batteries involving Zn anode. The results obtained here encourage the application of a similar water-in-salt strategy to revisit the electrochemistry of poorly performing reversible aqueous cells.

Conclusions

The electrochemistry of the delithiated tavorite-type VPO_4F was investigated vs. a metallic zinc anode in both wet ionic-liquid and aqueous zinc sulfate electrolytes. It was found that the delithiated VPO_4F is unstable when exposed to atmospheric moisture and is reduced gradually. This is believed to occur through proton insertion into the lattice and release of oxygen gas. The same H^+-insertion reaction is believed to be responsible for the observed electrochemical activity of the Zn – VPO_4F system, with moisture present in the electrolyte and the zinc metal acting, respectively, as a source of the H^+ ions and electrons. Furthermore, it was shown through elemental analyses that the insertion of Zn^{2+} into the VPO_4F host is not a favorable process, despite the high concentration of Zn^{2+} in the ionic-liquid electrolyte and the

elevated temperatures employed. Finally, it has to be emphasized that while water plays a critical role in enabling the redox chemistry in the Zn – VPO_4F system through the H^+ intermediate, utilization of aqueous electrolytes causes severe cathode-electrolyte dissolution that leads to extensive capacity loss and premature cell failure.

Conflicts of interest

There are no conflicts to declare.

Acknowledgments

This work was supported by the National Science Foundation grant DMR 1709081 and Welch Foundation grant F-1254.

References

1 M. Song, H. Tan, D. Chao and H. J. Fan, *Adv. Funct. Mater.*, 2018, **28**, 1802564.

2 P. Saha, M. K. Datta, O. I. Velikokhatnyi, A. Manivannan, D. Alman and P. N. Kumta, *Prog. Mater. Sci.*, 2014, **66**, 1–86.

3 R. J. Gummow, G. Vamvounis, M. B. Kannan and Y. He, *Adv. Mater.*, 2018, **30**, 1801702.

4 Y. Zhang, S. Liu, Y. Ji, J. Ma and H. Yu, *Adv. Mater.*, 2018, **30**, 1706310.

5 W. Kaveevivitchai and A. Manthiram, *J. Mater. Chem. A*, 2016, **4**, 18737–18741.

6 W. Kaveevivitchai, A. Huq and A. Manthiram, *J. Mater. Chem. A*, 2017, **5**, 2309–2318.

7 P. Canepa, G. Sai Gautam, D. C. Hannah, R. Malik, M. Liu, K. G. Gallagher, K. A. Persson and G. Ceder, *Chem. Rev.*, 2017, **117**, 4287–4341.

8 R. Y. Wang, B. Shyam, K. H. Stone, J. N. Weker, M. Pasta, H.-W. Lee, M. F. Toney and Y. Cui, *Adv. Energy Mater.*, 2015, **5**, 1401869.

9 J. Muldoon, C. B. Bucur and T. Gregory, *Chem. Rev.*, 2014, 114, 11683–11720.

10 R. Demir-Cakan, M. R. Palacin and L. Croguennec, *J. Mater. Chem. A*, 2019, **7**, 20519–20539.

11 D. Selvakumaran, A. Pan, S. Liang and G. Cao, *J. Mater. Chem. A*, 2019, **7**, 18209–18236.

12 G. Fang, J. Zhou, A. Pan and S. Liang, *ACS Energy Lett.*, 2018, **3**, 2480–2501.

13 H. Pan, Y. Shao, P. Yan, Y. Cheng, K. S. Han, Z. Nie, C. Wang, J. Yang, X. Li, P. Bhattacharya, K. T. Mueller and J. Liu, *Nat. Energy*, 2016, **1**, 16039.

14 F. Wan, L. Zhang, X. Dai, X. Wang, Z. Niu and J. Chen, *Nat. Commun.*, 2018, **9**, 1656.

15 W. Sun, F. Wang, S. Hou, C. Yang, X. Fan, Z. Ma, T. Gao, F. Han, R. Hu, M. Zhu and C. Wang, *J. Am. Chem. Soc.*, 2017, **139**, 9775–9778.

16 M. J. Park, H. Yaghoobnejad Asl, S. Therese and A. Manthiram, *J. Mater. Chem. A*, 2019, **7**, 7159–7167.

17 J.-M. Ateba Mba, C. Masquelier, E. Suard and L. Croguennec, *Chem. Mater.*, 2012, **24**, 1223–1234.

18 J. Wu, G. Gao, G. Wu, B. Liu, H. Yang, X. Zhou and J. Wang, *RSC Adv.*, 2014, **4**, 15014–15017.

19 J. Barker, M. Y. Saidi and J. L. Swoyer, *J. Electrochem. Soc.*, 2003, **150**, A1394.

20 A. P. Abbott, J. C. Barron, K. S. Ryder and D. Wilson, *Chem. - A Eur. J.*, 2007, **13**, 6495–6501.

21 Z. Liu, Q. Yang, D. Wang, G. Liang, Y. Zhu, F. Mo, Z. Huang, X. Li, L. Ma, T. Tang, Z. Lu and C. Zhi, *Adv. Energy Mater.*, 2019, **9**, 1902473.

22 M. V. Reddy, G. V. Subba Rao and B. V. R. Chowdari, *J. Power Sources*, 2010, **195**, 5768–5774.

23 M. Kim, S. Lee and B. Kang, *Adv. Sci.*, 2016, **3**, 1500366.

24 Y. Li, Z. Zhou, X. P. Gao and J. Yan, *J. Power Sources*, 2006, **160**, 633–637.

25 B. L. Ellis, T. N. Ramesh, L. J. M. Davis, G. R. Goward and L. F. Nazar, *Chem. Mater.*, 2011, **23**, 5138–5148.

26 H. Yaghoobnejad Asl and A. Choudhury, *RSC Adv.*, 2014, **4**, 37691–37700.

27 S.-D. Han, S. Kim, D. Li, V. Petkov, H. D. Yoo, P. J. Phillips, H. Wang, J. J. Kim, K. L. More, B. Key, R. F. Klie, J. Cabana, V. R. Stamenkovic, T. T. Fister, N. M. Markovic, A. K. Burrell, S. Tepavcevic and J. T. Vaughey, *Chem. Mater.*, 2017, **29**, 4874–4884.

28 H. Yaghoobnejad Asl and A. Manthiram, *Chem. Mater.*, 2019, **31**, 2296–2307.

29 C. J. Wen, B. A. Boukamp, R. A. Huggins and W. Weppner, *J. Electrochem. Soc.* , 1979, **126**, 2258–2266.

30 P. F. Xiao, M. O. Lai and L. Lu, *Solid State Ionics*, 2013, **242**, 10–19.

31 R. Ma, J. Shu, L. Shao, X. Lin, K. Wu, M. Shui, P. Li, N. Long and Y. Ren, *Ceram. Int.*, 2014, **40**, 15113–15119.

32 E. L. Smith, A. P. Abbott and K. S. Ryder, *Chem. Rev.*, 2014, **114**, 11060–11082.

33 V. Verma, S. Kumar, W. Manalastas, J. Zhao, R. Chua, S. Meng, P. Kidkhunthod and M. Srinivasan, *ACS Appl. Energy Mater.*, 2019, **2**, 8667–8674.

34 M. Yan, P. He, Y. Chen, S. Wang, Q. Wei, K. Zhao, X. Xu, Q. An, Y. Shuang, Y. Shao, K. T. Mueller, L. Mai, J. Liu and J. Yang, *Adv. Mater.*, 2018, **30**, 1703725.

35 K. W. Nam, H. Kim, J. H. Choi and J. W. Choi, *Energy Environ. Sci.*, 2019, **12**, 1999–2009.

36 B. Lee, C. S. Yoon, H. R. Lee, K. Y. Chung, B. W. Cho and S. H. Oh, *Sci. Rep.*, 2015, **4**, 6066.